


Laser shocking of nanocrystalline materials: Revealing the extreme pressure effects on the microstructural stability and deformation response

Cite as: Appl. Phys. Lett. **116**, 231901 (2020); <https://doi.org/10.1063/5.0008107>

Submitted: 18 March 2020 . Accepted: 15 May 2020 . Published Online: 08 June 2020

B. C. Hornbuckle , S. W. Dean, X. Zhou , A. K. Giri, C. L. Williams , K. N. Solanki , G. B. Thompson, and K. A. Darling

COLLECTIONS

 This paper was selected as Featured



View Online



Export Citation



CrossMark

Lock-in Amplifiers
up to 600 MHz



Laser shocking of nanocrystalline materials: Revealing the extreme pressure effects on the microstructural stability and deformation response



Cite as: Appl. Phys. Lett. **116**, 231901 (2020); doi: [10.1063/5.0008107](https://doi.org/10.1063/5.0008107)

Submitted: 18 March 2020 · Accepted: 15 May 2020 ·

Published Online: 8 June 2020



View Online



Export Citation



CrossMark

B. C. Hornbuckle,^{1,a)} S. W. Dean,¹ X. Zhou,² A. K. Giri,¹ C. L. Williams,¹ K. N. Solanki,³ G. B. Thompson,² and K. A. Darling¹

AFFILIATIONS

¹US Army CCDC Army Research Laboratory, Weapons and Materials Research Directorate, APG, Maryland 21005, USA

²Department of Metallurgical and Materials Engineering, University of Alabama, Tuscaloosa, Alabama 35487, USA

³School for Engineering of Matter, Transport, and Energy, Arizona State University, Tempe, Arizona 85287, USA

^{a)}Author to whom correspondence should be addressed: billy.c.hornbuckle.civ@mail.mil

ABSTRACT

We present the first results of laser-driven flyer plate experiments on a nanocrystalline copper-tantalum (NC-Cu-Ta) alloy. A pulsed Nd:YAG laser (1.2 J/pulse, 10 ns) is used to accelerate an Al foil disk ($25\ \mu\text{m} \times \sim 800\ \mu\text{m}$) off a glass substrate at velocities of 0.8 and 2.4 km/s through a small air gap and impact the NC-Cu-Ta target. The flyer velocities were determined from a high-speed video and extensive post-impact analyses were conducted using advanced electron microscopy revealing the formation of a band structure leading to a non-trivial upper bound for the breakdown of an extremely stable NC-microstructure and physical-properties.

© 2020 Author(s). All article content, except where otherwise noted, is licensed under a Creative Commons Attribution (CC BY) license (<http://creativecommons.org/licenses/by/4.0/>). <https://doi.org/10.1063/5.0008107>

Laser-driven flyer plates represent a low-cost, high-throughput method to induce highly shocked states in a target for short durations, on the order of nanoseconds. This technique provides the opportunity to investigate new structural materials that display anomalous mechanical and physical properties under such conditions.¹ Conventional shock recovery experiments using flyer plates accelerated to high velocities in gas guns have been instrumental in understanding the structure-property relationships in metals when shocked to a high Hugoniot compressed state.² For instance, depending on the peak pressure that is generated, pressure rise time, and pulse duration, the microstructure of most metals/alloys will evolve to contain a high concentration of defects, i.e., dislocations, point defects, and/or deformation twins resulting in an extreme strain-rate dependent behavior.³ Additionally, some structural alloys, such as titanium alloys, have been shown to undergo a pressure-induced phase transformation.⁴ The generation and evolution of such shock-induced defects in metals, as observed post-mortem, have been correlated to provide insight to their physical response and failure.⁵ All the same, the practical limitation of recovering samples having experienced very high-pressure states

(>30 GPa) has limited the available knowledge of the substructures which develop from hyper velocity impacts. Therefore, for strain-rates ranging from 10^6 to $10^7\ \text{s}^{-1}$, the deformation mechanisms are less well understood, especially for bulk nanocrystalline (NC) alloys where conventional deformation mechanisms may not be applicable.⁶

Laser-driven flyer plates, produced by laser-plasma acceleration of thin metal foils adhered to a glass substrate, could be a method to access such extreme regimes in NC materials, along with any transition in the deformation mode (slip vs twinning). In this Letter, a systematic study of laser-driven flyer plate impacts (using flyer plates of Al) at velocities ranging from 0.8 km/s to 2.4 km/s in NC copper-tantalum [Cu-3Ta (at.%)] is presented. Recently, Darling and colleagues have shown that the immiscible NC-Cu-Ta alloy system is not only thermally stable⁷ but also thermo-mechanically stable.^{8–15} Previously, the mechanical response of these types of alloys has been reported under various strain-rate conditions, ranging from 10^{-8} to $10^5\ \text{s}^{-1}$ ^{19,16} and shown to exhibit minimal defect evolution post-mortem.⁹ Therefore, this work explores the physical mechanisms and structural stability at play in a NC-Cu-3Ta (at.%) alloy by

laser-driven (Al) flyer plate impact, i.e., beyond the strain-rate of 10^5 s^{-1} . The tested specimens will then have their microstructures characterized via scanning transmission electron microscopy (STEM) to elucidate microstructural stability and deformation mechanisms. In addition, this alloy provides a unique opportunity for the NC community to expand its knowledge base into one of the remaining and relatively unexplored areas of extreme strain rates in NC metals.

Toward this, a series of stabilized NC-Cu-3Ta (at.%) disks 3 mm in diameter and ~ 0.5 mm in thickness were produced from mechanically alloyed powders using multi-pass high temperature equal channel angular extrusion (ECAE) at 700°C . Complete details of the powder processing and consolidation efforts can be found in Refs. 8–15. Preliminary microstructural analysis of the as-consolidated test samples using STEM (Fig. 1) indicates that the extruded microstructure for this alloy had an average grain size of 89 nm. Prior statistical analysis revealed the presence of an extremely dense network of Ta based nanoclusters with a mean diameter of 2 nm within the microstructure.^{17,18} These nanoclusters exist within the Cu matrix and along grain boundaries, as shown in Fig. 1. It has been previously determined that such nanoclusters play an important role in dictating the mechanical response as well as stabilizing the matrix grain size under the application of stress and temperature, such as during processing and high rate mechanical testing.^{9,13,16} To evaluate microstructural stability under extreme rates, the NC-Cu-3Ta (at.%) disks were impacted by laser-driven flyer plates at 0.8 km/s (~ 9 GPa shock pressure) and 2.4 km/s (~ 34 GPa shock pressure). Flyer velocities were determined from a high speed video or multi-flash imaging. In multi-flash imaging, a single long exposure is taken, while a light source is rapidly pulsed. In these experiments, the light source is a spoiled-coherence illumination laser (646 nm, 6 ns pulse length, 10 MHz repetition rate). The laser was pulsed seven times to build up an image showing the development of the plate over time. The change in the position of the leading edge of the plate was used with the known repetition rate of the laser to determine the plate's velocity. A schematic of the flyer launch system and a multi-flash image of a low velocity experiment are shown in Fig. 2. In addition, a supplemental movie has been provided in the [supplementary material](#) of the flyer forming and impacting the surface of the prepared NC-Cu-3Ta sample.

As is apparent in the inset image in Fig. 2, the laser-driven flyer plate is not flat, as is generally the case in gas gun experiments. The spatial energy profile of the launch laser determines the plate

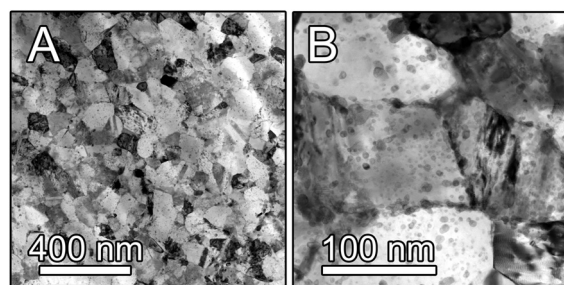


FIG. 1. Bright field (BF) STEM image of the as-received (i.e., post ECAE processed) sample. (a) Low magnification image showing the Cu grain structure. (b) High magnification BF STEM images showing the high density of Ta based clusters residing in the lattice as well as along the grain boundaries of the Cu based matrix.

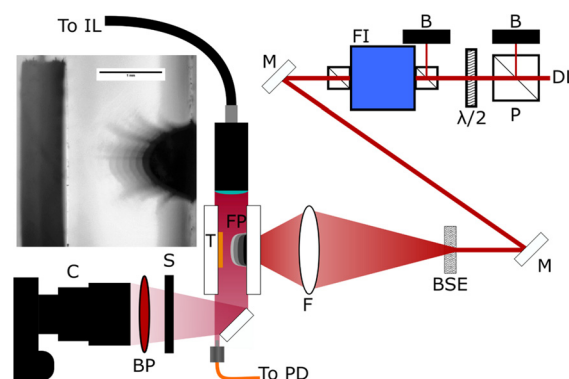


FIG. 2. Laser-driven flyer plate launch and multi-flash imaging system. DL = drive laser, B = beam block, P = polarizing beam cube, $\lambda/2$ = half-wave plate, FI = Faraday isolator, M = mirror, BSE = beam-shaping element, F = focusing lens, FP = flyer plate, T = target, S = fast mechanical shutter, BP = bandpass filter, C = camera, PD = photodiode. The inset is an example multi-flash image of flyer launch. The image was taken with seven, 6 ns illumination pulses fired at 10 MHz (see the [supplementary material](#) for a live movie).

geometry. In the case of the system used here, this profile is approximately Gaussian, as determined by both the beam profile out of the laser and the effect of the beam-shaping element used to modify the beam. A small enough area under the tip of the plate, however, will see the plate as effectively flat. As the microstructural analysis presented in this paper deals with a very small area directly at the point of this impact, it is assumed that the impact is one-dimensional (1D). This assumption greatly simplifies analysis, but obviously does not capture the full complexity of the impact event. However, the values determined using this assumption provide estimates for the true shock state experienced by the analyzed volume of the sample (refer to the [supplementary material](#)). Nevertheless, laser-driven flyer plates are not a replacement for gas-gun experiments, but due to their vastly lower cost, they can reduce the number of such large-scale experiments needed by providing a rough map of interesting states to explore.

Extensive post-impact analysis was conducted on the targets utilizing advanced electron microscopy. An example of a crater generated by the flyer plate impacting on the surface of the NC-Cu-3Ta (at.%) disk is provided in [supplementary material](#) Fig. S1. The low magnification scanning electron micrographs of the impacted area indicate that the short duration shocks generated by laser-driven flyer were sufficient to induce changes in the materials. As seen, residual Al leftover from the flyer was identified on the surface of the disk. On the macroscopic scale, the rest of the sample appears undamaged, with no cracks propagating outward from the impact site or embrittlement causing the sample to break up into smaller pieces. The perimeter of the impact site is encircled by a rim of deep gouges. These gouges are thought to be caused by erosion from plasma jets that surround the flyer plate, and are a result of the launch process. From the center of the impact site (marked with a red circle), the TEM specimen was extracted using the site-specific lift-out technique via a focused ion beam (FIB) from the middle of the crater. This TEM foil preparation was duplicated for the sample impacted at 0.8 km/s. The entire TEM foil for both impacted samples (2.4 and 0.8 km/s) is provided in [supplementary material](#) Fig. A2. The composite STEM Bright Field images provide a look at $\sim 50 \mu\text{m}^2$ of electron transparent

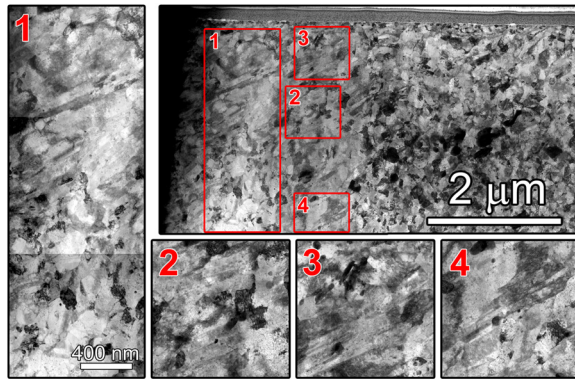


FIG. 3. Composite STEM (bright) field images providing a closer look at the microbanded regions of the microstructure that underwent laser-driven flyer plate shock at 2.4 km/s (34 GPa). The micro-bands occur sporadically, i.e., in only a few, isolated places throughout the microstructure with an average spacing of ~ 120 nm.

microstructure for each sample. Initial STEM analysis of the samples found that the flyer plate impact at 2.4 km/s resulted in the formation of microbands roughly $1 \mu\text{m}$ from the impact surface, as shown in Fig. 3 (a high magnification of [supplementary material Fig. S2](#)), while the majority of the remaining microstructure is unaffected by the pressure generated during impact (comparison to as-received, Fig. 1). Furthermore, the 2.4 km/s sample revealed that the microbands extend over a micrometer or two and are discontinuous throughout the microstructure. From Fig. 3, it is evident that the microbands consist of laminar structures, which at first glance appear to be consistent with nanotwins intermixed with microbands (in which regions of elevated dislocation density, resulting in polygonization and cell wall

structures). Besides the microbands and a few dislocations, the microstructure is free of damage with no cracking or de-bonding of interfaces observed. Furthermore, the insensitivity to shock was also observed in the sample impacted at 0.8 km/s, whereby the entire microstructure remained indistinguishable from the as-received condition.

A closer look at the un-deformed regions of the 2.4 km/s sample reveals the microstructure to be very resilient to the extreme pressures generated during shock impulse loading. The shock pressure was calculated to be 9 and 34 GPa for 0.8 and 2.4 km/s velocity impacts, respectively. The Cu grain size and size distributions in Figs. 4(a) and 4(b) show very little change in either, despite being successfully shock compressed to a stable high-pressure Hugoniot state. The grain size remains equiaxed in shape and increases from $89 \text{ nm} \pm 41 \text{ nm}$ in the as-received to $179 \pm 117 \text{ nm}$ after shock loading at 2.4 km/s, the most extreme case. Such small changes in microstructure are very surprising given that the average grain size is less than 200 nm and experienced pressures as high as 34 GPa along with temperature rises to 526 K (calculated during impact). In contrast, Lu *et al.* observed a rapid grain coarsening from 70 nm to 800 nm in pure nanocrystalline Ta when subjected to a laser pulse with an energy of 684 J.¹⁹ Higher magnification STEM was used to resolve the underlying microstructural features in more detail. [supplementary material Figs. 3\(a\)–3\(d\)](#) illustrate that the Ta nanoclusters are distributed homogeneously in the grain interiors and at grain boundaries and interact with dislocations. Despite the high number density of Ta nanoclusters, no obvious voids or debonding from the matrix was observed. The average size of the nanoclusters was found to be $\sim 2\text{--}4 \text{ nm}$ in diameter with an average inter-nanocluster spacing of $5.23 \pm 1.74 \text{ nm}$. These numbers remain nearly constant with the application of high state of stress, highlighting the alloy stability and resistance to coarsening under the extreme loading conditions. It is owing to the stability and high density of the coherent

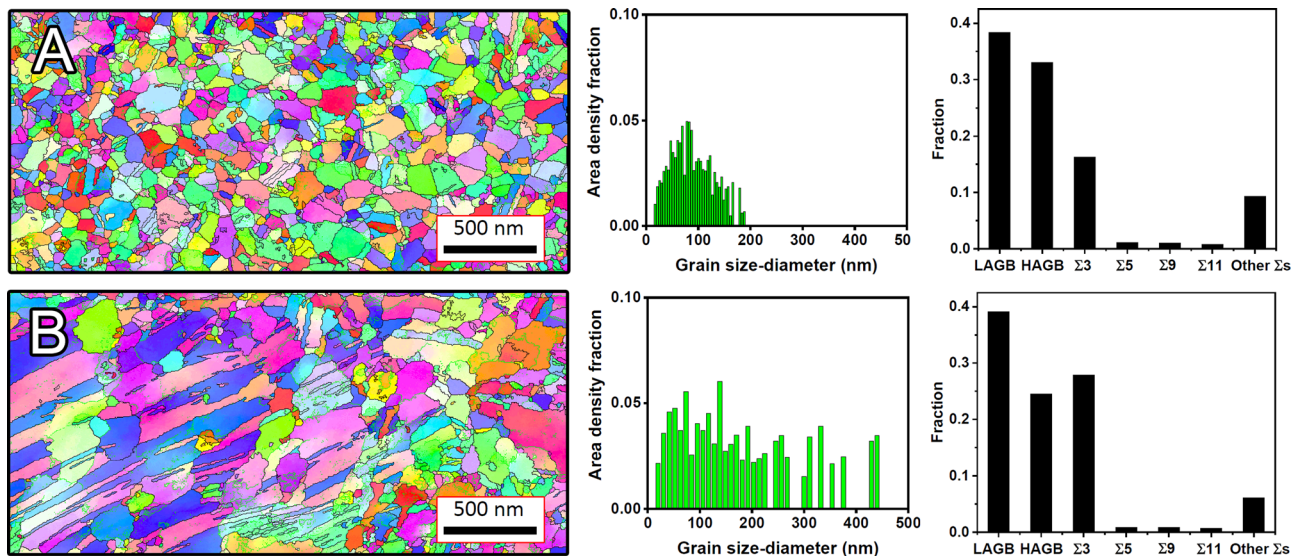


FIG. 4. Microstructural data acquired for as-received and shock compressed bulk NC-Cu-3 at. % Ta alloy using Precession Electron Diffraction (PED) microscopy. Precession diffraction image along with the grain size distribution plot and finally the distribution plot for the characteristic grain boundary types for the (a) as-received material and (b) material shock compressed using the laser flyer plate to ~ 34 GPa. The distributions indicate a nominal increase in Cu grain size with the majority of the grains remaining in the NC regime as compared to a rapid grain coarsening from 70 nm to 800 nm in pure nanocrystalline Ta when subjected to a laser pulse with energy of 684 J.¹⁹

nanoclusters present in the microstructure that the Cu grains remain almost intact. These observations suggest that the nanoclusters pin the grain boundaries and block the grain boundary sliding and grain rotation processes.¹³

To evaluate the influence of the deformation rate on the textural changes (grain boundary sliding and grain rotation processes), precession diffraction measurements were performed in various regions. The orientation imaging map (OIM) shows a high degree of randomness in the orientation relationships between the Cu grains in the as-received state with a texture index of 2.4, see Fig. 4. However, for the microbands intermixed with twins in the 2.4 km/s impacted sample, the local texture is quite significantly different with a texture index of 9.1. This effect is due to the deformation experienced in the sample impacted at 2.4 km/s within these localized regions. Further analysis of the microband region indicates that the sigma three boundary types have roughly doubled in number fraction. In addition, only a marginal change in the average grain size was observed between the as-received sample and the shock recovered samples, i.e., the average grains are still in the nanoscale as compared to ~1140% observed for pure nanocrystalline Ta under similar loading conditions.¹⁹ This is true even for the ~34 GPa sample where the vast majority of the microstructure remains relatively un-coarsened (see Fig. 4).

Under shock conditions, FCC metals with high stacking fault energies' (SFE's) such as pure Cu and NC Cu-Ta alloys form a mixture of nanotwins and microbands. As grain size decreases the stress/pressure required to form deformation-twins increases significantly, and therefore, the observed volume fraction should go down. Further, in the case of NC-Cu-3Ta alloy, there is an active competition between dislocation motion and twinning to decide which will be the more operative deformation mechanism at high-rates.²⁰ Along the same line, in our previous work, we used the generalized stacking fault energy (GSFE) curves to measure and understand the competition between dislocation slip and twinning, often referred to as the *twinnability* of the material.^{20,21} The ratio of the unstable twinning fault energy to the unstable stacking fault energy, $\beta = \gamma_{uf} / \gamma_{usf}$, was used to explain the role of Ta in deformation twinning in NC Cu-Ta alloys. For pure Cu, the ratio β is close to unity (~1.11), i.e., the energy barrier for a twin fault is smaller and hence, nucleating a twin fault is relatively easy. However, as the value of β increases, the energy barrier as well as the stress required to nucleate twins increases. In the case of NC-Cu-Ta, a ratio of 1.18 was found indicating similar deformation mechanisms as compared to that of a pure coarse-grained Cu. However, the critical pressure for twinning is significantly different from that for pure Cu, indicating the role of grain size. For instance, the minimum twinning pressure for coarse-grained Cu and Cu alloys is in the range of 14–20 GPa.^{21,22} The minimal amount of twinning observed in nanocrystalline Cu-Ta is an indicator of the higher threshold pressure required to induce twinning at these smaller grain sizes.

To further investigate the stability of the microstructure under such extreme conditions, we probed the residual hardness using a micro-hardness indenter. The hardness was measured from various spots within the impact crater using 100 g load, which resulted in an average diagonal length of 13 μm . Given the geometry of Vickers indenters, this equated to an analysis depth of 1.9 μm . Changing the load to probe a range in depth (1–3.5 μm) provided consistent results. The average value for the hardness was found to be 2.68, 2.40, and 2.54 GPa at a shocked pressure of 9, 24, and 34 GPa, respectively. Comparing

these values with 2.48 GPa value for the as-received condition indicates negligible change in the residual hardness for the NC-Cu-Ta alloy. In contrast, Lu *et al.* observed a ~50% increase in pure nanocrystalline Ta strength when subjected to a laser pulse with an energy of 684 J.¹⁹ A similar increase in the relative hardness (30% increase) was observed when nanocrystalline Ni was subjected to a shock pressure of 40 GPa.²³ Overall, the lack of accumulated defect structures such as the formation of cell structures (indicative of high dislocation density) within the microstructure of NC-Cu-Ta alloys, as shown in Fig. 3, bodes reasonably well with the post-deformed hardness measurements.

In summary, the extreme conditions of laser-driven flyer plate shock at high velocities provide a first look into the dynamic breakdown of these thermo-mechanically stable NC Cu-Ta alloys. Initial results indicate that the short duration shocks caused by plate impact was sufficient to induce small changes in the structure of the sample, through the appearance of microbands composed primarily of nanotwins and microbanding at very high velocities and pressures. However, the microstructures remain unaffected and free from damage accumulation at moderate shock velocities and pressures. These findings demonstrate that stable nanocrystalline microstructures have a high tolerance for defect accumulation under compressing shock loading. This indicates that such metals may have enhanced physical and mechanical properties for impact and ballistic protection and mitigation.

See the [supplementary material](#) for the equations used to determine the experimental conditions in the shocked nanocrystalline Cu-3Ta (at.%) material. Additionally, the laser-driven Al flyer plate impact parameters used in the shock analysis as well as the resulting calculated shock values are listed in Tables S1 and S2. Low and higher magnification SEM micrographs showing the impact surface for the highest and lowest impact shock velocities can be seen in Fig. S1. Composite STEM bright field images for the entire TEM liftouts of the highest and lowest impact velocities are included as Fig. S2 to provide a macro view of the shocked microstructures. Finally, low and higher magnification STEM bright field images highlighting the grain structure, Ta clusters, and dislocations within the shocked microstructures compose Fig. S3.

The authors acknowledge A. J. Roberts and T. Luckenbaugh for the synthesis of the Cu-Ta powder; T. Luckenbaugh, S. Marsh, and M. C. Aniska for consolidation of the Cu-Ta powder and machining. K.N.S. acknowledges the support of U.S. Army Research Laboratory and the National Science Foundation under Contract Nos. W911NF-15-2-0038 and 1663287. X.Z. and G.B.T. gratefully acknowledge No. NSF-DMR-1709803 for support.

The authors declare no competing financial interest.

DATA AVAILABILITY

The raw/processed data required to reproduce these findings are available within the article [and its [supplementary material](#)].

REFERENCES

- ¹A. D. Curtis, A. A. Banishev, W. L. Shaw, and D. D. Dlott, *Rev. Sci. Instrum.* **85**, 043908 (2014).
- ²M. A. Meyers, *Dynamic Behavior of Materials* (John Wiley & Sons, 1994).
- ³M. A. Meyers, F. Gregori, B. K. Kad, M. S. Schneider, D. H. Kalantar, B. A. Remington, G. Ravichandran, T. Boehly, and J. S. Wark, *Acta Mater.* **51**, 1211 (2003).

- ⁴E. Cerreta, G. T. Gray, A. C. Lawson, T. A. Mason, and C. E. Morris, *J. Appl. Phys.* **100**, 013530 (2006).
- ⁵C. L. Williams, *Synthesis SEM Lectures Experimental Mechanics* (Morgan & Claypool, 2019), Vol. 2, p. 1.
- ⁶V. Yamakov, D. Wolf, S. R. Phillpot, A. K. Mukherjee, and H. Gleiter, *Nat. Mater.* **3**, 43 (2004).
- ⁷K. A. Darling, A. J. Roberts, Y. Mishin, S. N. Mathaudhu, and L. J. Kecskes, *J. Alloys Compd.* **573**, 142 (2013).
- ⁸K. A. Darling, M. Rajagopalan, M. Komarasamy, M. A. Bhatia, B. C. Hornbuckle, R. S. Mishra, and K. N. Solanki, *Nature* **537**, 378–381 (2016).
- ⁹S. A. Turnage, M. Rajagopalan, K. A. Darling, P. Garg, C. Kale, B. G. Bazezhour, I. Adlakha, B. C. Hornbuckle, C. L. Williams, P. Peralta, and K. N. Solanki, *Nat. Commun.* **9**, 2699 (2018).
- ¹⁰K. A. Darling, M. A. Tschopp, R. K. Guduru, W. H. Yin, Q. Wei, and L. J. Kecskes, *Acta Mater.* **76**, 168 (2014).
- ¹¹K. A. Darling, E. L. Huskins, B. E. Schuster, Q. Wei, and L. J. Kecskes, *Mater. Sci. Eng., A* **638**, 322 (2015).
- ¹²B. C. Hornbuckle, T. Rojhirunsakool, M. Rajagopalan, T. Alam, G. P. P. Pun, R. Banerjee, K. N. Solanki, Y. Mishin, L. J. Kecskes, and K. A. Darling, *JOM* **67**, 2802 (2015).
- ¹³R. K. Koju, K. A. Darling, K. N. Solanki, and Y. Mishin, *Acta Mater.* **148**, 311 (2018).
- ¹⁴K. A. Darling, C. Kale, S. Turnage, B. C. Hornbuckle, T. L. Luckenbaugh, S. Grendahl, and K. N. Solanki, *Scr. Mater.* **141**, 36 (2017).
- ¹⁵M. Rajagopalan, K. Darling, S. Turnage, R. Koju, B. Hornbuckle, Y. Mishin, and K. Solanki, *Mater. Des.* **113**, 178 (2017).
- ¹⁶C. Kale, S. Turnage, P. Garg, I. Adlakha, S. Srinivasan, B. C. Hornbuckle, K. Darling, and K. N. Solanki, *Mater. Des.* **163**, 107551 (2019).
- ¹⁷B. C. Hornbuckle, C. Kale, S. Srinivasan, T. L. Luckenbaugh, K. N. Solanki, and K. A. Darling, *Scr. Mater.* **160**, 33 (2019).
- ¹⁸V. H. Hammond, T. L. Luckenbaugh, M. Aniska, D. M. Gray, J. A. Smeltzer, B. C. Hornbuckle, C. J. Marvel, K. N. Solanki, T. Schmitz, and K. A. Darling, *Adv. Eng. Mater.* **20**, 1800405 (2018).
- ¹⁹C. H. Lu, B. A. Remington, B. R. Maddox, B. Kad, H. S. Park, M. Kawasaki, T. G. Langdon, and M. A. Meyers, *Acta Mater.* **61**, 7767 (2013).
- ²⁰M. Bhatia, M. Rajagopalan, K. Darling, M. Tschopp, and K. Solanki, *Mater. Res. Lett.* **5**, 48 (2017).
- ²¹T. Cai, Z. J. Zhang, P. Zhang, J. B. Yang, and Z. F. Zhang, *J. Appl. Phys.* **116**, 163512 (2014).
- ²²J. C. Sanchez, L. E. Murr, and K. P. Staudhammer, *Acta Mater.* **45**, 3223 (1997).
- ²³Y. M. Wang, E. M. Bringa, J. M. McNaney, M. Victoria, A. Caro, A. M. Hodge, R. Smith, B. Torralva, B. A. Remington, C. A. Schuh, H. Jamarkani, and M. A. Meyers, *Appl. Phys. Lett.* **88**, 061917 (2006).